DOI: https://doi.org/10.37434/tpwj2025.02.07

DETECTION OF CIRCULAR SUBSURFACE DEFECTS IN LAMINATED COMPOSITES USING OPTICAL-ACOUSTIC NONDESTRUCTIVE TESTING SYSTEM

O.M. Sharabura, L.I. Muravsky, O.G. Kuts

G.V. Karpenko Physico-Mechanical Institute of the NASU
5 Naukova Str., 79060, Lviv, Ukraine

ABSTRACT

An optical-acoustic system layout for nondestructive testing of subsurface defects in laminated composites has been developed. Detection and localization of subsurface defects in composite laminated structures with the help of the optical-acoustic system layout are performed by forming a series of dynamic speckle patterns of the composite surface, which is excited by a flexural elastic wave, their subsequent recording and accumulation in order to generate differential digital speckle patterns and extract optical spatial responses from defects. To assess the efficiency of detecting such defects, fiberglass laminated structures were manufactured containing three layers of glass textolite plates and circular flat defects of various sizes in the middle layer. Based on the conducted studies, an experimental dependence of the fundamental resonance frequency of circular subsurface defects on their sizes was obtained, which is close to the theoretically plotted one. It is shown that using the created optical-acoustic system layout, it is possible to detect such defects in a wide range of changes in their sizes.

KEYWORDS: optical-acoustic system, dynamic speckle pattern, circular subsurface defect, region of interest, difference speckle pattern, elastic wave, laminated composite

INTRODUCTION

Constant improvement of materials and structural elements, used in mechanical engineering, aerospace, construction industry, etc. requires continuous development of methods and means of their nondestructive testing (NDT) and technical diagnostics. In order to develop new and improve the available methods of NDT of materials and structures, processes of different physical nature, are used. A lot depends on the conditions, under which the control process is expected to be carried out, properties of materials, from which the object of study is made, types of defects to be revealed, etc. Over the recent years, high-speed NDT equipment has been intensively developed. It is based on the principles of thermography, digital speckle-interferometry and shearography [1–4] and enables parallel selection of 2D and 3D data arrays from a large area of the object of study and their further digital processing.

The advantage of thermographic methods is the large area of the object and contactless procedure of material heating. Their possibilities, however, are limited by the small thickness of the material of the object of study, considerable energy costs for its heating and high cost of equipment, in particular an infrared camera. Moreover, the need for preheating the object of study is harmful to the environment and worsens the ecological condition of the surrounding area.

Shearography methods are effectively used for NDT of surfaces of a large area [3–6]. Shearography systems allow testing a large area of the object of study with a high speed without any need for additional heating. They are applied to detect, measure and localize anomalies by reproduction and visualization of microscopic changes on the studied surface during the respective loading. The digital shearography camera checks the entire field of vision practically simultaneously, in contrast to vibrometric and ultrasonic (US) scanning means of [3]. There exist a range of methods of loading application in such systems, in particular diverse mechanical and vibrational loads, loading under the impact of sonic or US signals, pressure, etc., which lead to minor local deformations of the surface caused by both surface and subsurface defects. These can be impact damage, disbanding delamination, porosity, thermal damage, cracks, etc. Such deformations are readily identified by NDT shearography systems [1, 2, 5, 6]. In such systems, however, it is necessary to use a complex imaging module, which complicates their overall design.

Unlike the interferometry NDT methods, in the optical-acoustic method (OAM) only the speckle patterns of the surface are used to detect subsurface defects in composite structures. The surface is excited by elastic waves from an acoustic radiation source. Coherent speckle patterns are formed without application of a reference laser beam, resulting in considerable simplification of optical-digital NDT systems, implementing OAM. The method consists in exciting a composite structure with a flexural elastic wave, illuminating an area of the composite surface with an expanded laser beam, and forming a series of dynamic speckle patterns of the composite surface area generated with opposite polarities of the elastic wave, the frequency of which changes monotoni-

cally. A digital camera accumulates two series of dynamic speckle patterns and, as a result of this accumulation, records a pair of digital speckle patterns (DSPs). After high-speed processing of the DSP pairs, defect maps are obtained containing optical spatial responses from regions of interest located directly above the defects. Further, the obtained defect maps are used to determine the location, dimensions and depth of occurrence of subsurface defects. OAM is described in detail in works [7–11].

OPTICAL-ACOUSTIC SYSTEM FOR NONDESTRUCTIVE TESTING OF SUBSURFACE DEFECTS

A layout of optical-acoustic system (OAS) for subsurface defects NDT was created for OAM technical realization [7–11]. Its block-diagram is shown in Figure 1. One of the key points of difference of OAS consists in that compared to the known interferometry systems for internal defects detection it does not contain an interferometer or a shearography unit. Due to that it has a much simpler design and low sensitivity to vibrations and other external impacts.

Optical spatial response from a subsurface defect to OAS is generated by comparing the recorded DSP $I_{n1}(i, j)$ obtained at maximum values of elastic wave amplitude, with DSP $I_{n2}(i, j)$ obtained at their minimum values. The procedure of DSP cross-correlation is described in detail in [9–11] and it is performed by deriving the difference DSP:

$$I_n(i,j) = |I_{n1}(i,j) - I_{n2}(i,j)|. \quad (1)$$

After deriving the difference DSP which can be interpreted as a defect map, a natural question arises, how the defect parameters can be determined based on the generated map. For this purpose, we need to establish a connection between the subsurface defect shape and its size and depth of occurrence. One of the possible approaches to solving this problem consists in application of mathematical physics methods for construction of a mathematical model of the respective defect. To derive the expressions, connecting the physical parameters of the material, from which the diagnosed object is made, with the defect parameters and its resonance frequencies, the approaches developed for the theory of plates and shells are applied [12, 13]. The works, analyzed and generalized in [13], present the research results for flat isotropic and anisotropic plates of different shape, in particular for rectangular [14, 15], round and elliptical [16–19] ones, including those with different boundary conditions. The theory of vibrations of plates and shells [12, 13] in different recording variants is widely used in the field of nondestructive testing and technical diagnostics [20–24]. In [9–11], in particular, the formulas for

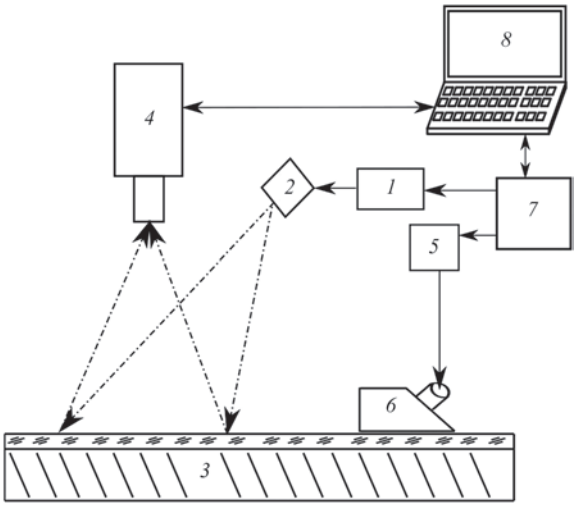

Figure 1. Simplified optical schematic of OAS layout: *1* — semiconductor laser with amplitude modulation; *2* — laser beam expander; *3* — fiberglass laminated structure, containing layers of STEF-1 glass textolite and subsurface defects in the middle layer; *4* — digital camera with a lens; *5* — broadband signal generator for piezoelectric converter; *6* — piezoelectric converter; *7* — control unit; *8* — computer

the model of a square subsurface defect are used. According to this model, the region of interest above the planar defect can be regarded as a thin square membrane, clamped at the edges. If such a defect is excited in one of its resonance frequencies, i.e. in one of the resonance frequencies of the region of interest above the defect, then an optical spatial response from the defect will form at OAS output. For a circular planar subsurface defect, a model of a circular plate from an isotropic material clamped at the edges, can also be used, which can be regarded as the region of interest above the subsurface defect, the dimensions of which correspond to the defect dimensions. According to [13, 20], the formula for determination of fundamental frequency f_{01} of resonance vibration of such a plate has the following form:

$$f_{01} = 0.47 \frac{h}{a^2} \sqrt{\frac{E}{\rho(1-\nu^2)}}, \quad (2)$$

where a is the membrane radius, mm; h is the depth of defect occurrence, mm; E is the Young's modulus, GPa; ρ is the material density, kg/m^3; ν is the Poisson's ratio.

EXPERIMENTAL STUDIES

Experimental studies on detection and identification of subsurface circular planar defects were conducted on samples of fiberglass laminated structures of 400×250 mm size, each of which was produced from three plates of STEF-1 glass textolite and epoxy phenolic polymer resin as a binder [10]. The lower layer, a 5 mm plate from STEF-1 glass textolite provided the structure rigidity. A series of circular and square

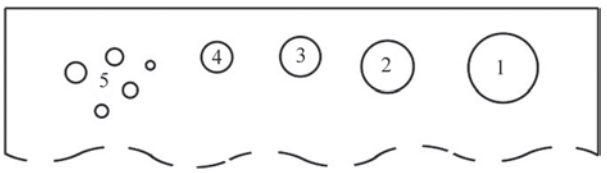

Figure 2. Schematic of arrangement of circular subsurface defects in the detected section of sample No. 1 of the fiberglass laminated structure and their diameters, mm: 1 — 45; 2 — 35; 3 — 25; 4 — 20; 5 — a group of five defects with diameters of 14, 12, 10, 8, 6 mm

holes were cut out in the middle layer, in 1.5 mm glass textolite plate. Made from the same material upper layers in the samples have different thickness. In sample No. 1 from fiberglass laminated structure, which was studied, the upper layer is 0.41 mm thick, i.e. the depth of defect occurrence in this sample is $h = 0.41$ mm. Figure 2 shows the scheme of arrangement of circular subsurface defects in the highlighted section of sample No. 1 with the thickness of upper glass textolite plate $h = 0.41$ mm, numbered from 1 to 5 in the order of decreasing defect diameters.

The developed OAS layout implements a method of quick real-time testing of the studied surface. For this purpose, after setting all the required parameters of the system, we analyze the difference DSP in a wide range of variation of the frequency of the sample excitation by an elastic wave. Each difference DSP is analyzed pixel by pixel for exceeding a certain preset noise level (NL) and under the condition of its exceeding in a certain image pixel, we record this event with a counter. After such verification we obtain M pixels with excess noise level for each difference DSP and for each preset excitation frequency. Further on we will divide this number by the total number of pixels in the image, and as a result we obtain the percentage of the area of optical spatial response from the region of interest, which exceeds the noise level, and, thus, can contain the subsurface defect. During this procedure, the difference DSP is saved for each excitation frequency, in case of exceeding the NL. Derived difference DSP is further on analyzed and processed using the simplest algorithms for digital image processing (DIP).

During NDT of sample No. 1 the difference DSP of the sample surface were obtained using OAS layout and optical spatial responses from defects No. 1–4 were analyzed in the range of variation of piezoelectric converter frequency of 1–50 kHz. Figure 3 shows the difference DSPs after application of DIP procedure, where optical responses from circular defects of different diameters are clearly visible.

Analysis of the images in Figure 3 allows following the correlation of the optical response areas and the respective defect areas, the area of responses from defects becoming smaller with reduction of their sizes. So, for instance, Figure 3, *a* gives an optical response from subsurface defect No. 1, 45 mm in diameter at resonance frequency $f_{01} = 1.8$ kHz. Figure 3, *b* shows the optical response from defect No. 2, 35 mm in diameter at resonance frequency $f_{01} = 2.8$ kHz. However, response from circular defect No. 3 (Figure 3, *c*) at resonance frequency $f_{01} = 4.6$ kHz is much smaller than its diameter, which is attributable to a too weak response from the sample surface, caused by a considerable distance between the excitation source and this defect. Therefore, to obtain defect map from the rest of test defects, the excitation source was moved closer to their location. Figure 3, *d* shows the optical response from a defect 20 mm in diameter at resonance frequency $f_{01} = 7.6$ kHz, the size of which is also smaller than the defect size. Despite the absence of the possibility of accurate determination of the radius of circular subsurface defect, evaluation of its size is satisfactory and sufficient for NDT objectives. Figure 4 gives improved defect maps for defect group No. 5. Figure 4, *a*, *b*, *c* shows the sample surface area where four of five defects of group No. 5 are concentrated, including the largest defect 14 mm in diameter (Figure 4, *a*) obtained at resonance frequency $f_{01} = 13.8$ kHz. The smallest defect 6 mm in diameter from defect group No. 5 could not be seen in the studied frequency range. In Figure 4, *b* we can simultaneously see defects 12, 10 and 8 mm in diameter at resonance frequency $f_{01} = 21.6$ kHz. At this frequency the largest response is formed by a defect 12 mm in diameter. Figure 4, *c* shows the optical response from a defect 8 mm in diameter at frequency $f_{01} = 35.8$ kHz.

Figure 5 presents the theoretical (curve *1*) and experimental (curve *2*) curves of the dependence of resonance frequency f_{01} on the sizes of subsurface defects in sample No. 1. The numbers mark the experimental data obtained for circular defects numbered in Figure 2. To derive a theoretical dependence (curve *1*) formula (*2*) was used, where the parameter

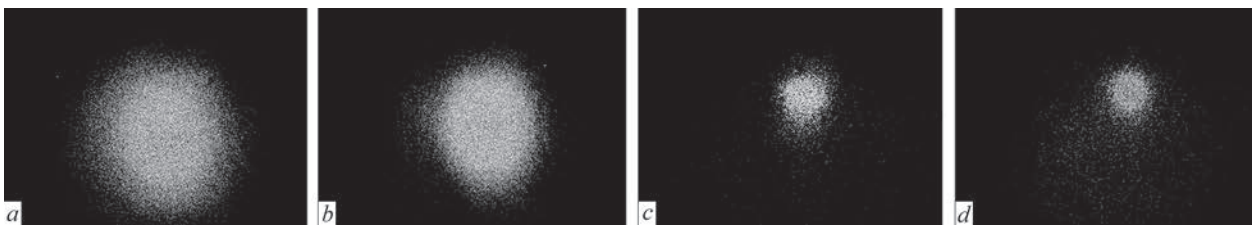

Figure 3. Optical spatial responses from subsurface defects No. 1 — 45 mm in diameter (*a*), No. 2 — 35 (*b*), No. 3 — 25 (*c*), No. 4 — 20 (*d*), which became visible in defect maps

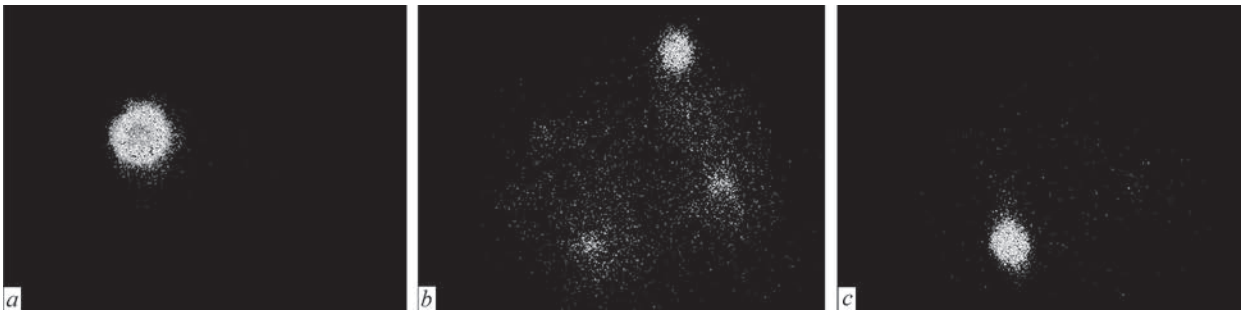

Figure 4. Defect maps of subsurface defect group No. 5 (Figure 2), recorded at the highest intensity of optical responses from defects with diameters of 14 (*a*), 12 (*b*), 8 mm (*c*)

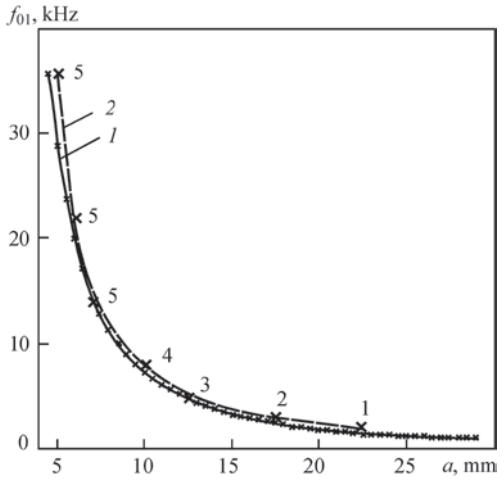

Figure 5. Theoretical (*1*) and experimental (*2*) dependencies of resonance frequency f_{01} on circular defect radius *a*

values were taken from [10] based on experimental data for STEF-1 glass textolite plate. Here the depth of defect occurrence h = 0.41 mm, modulus of elasticity E = 23.3±1.3 GPa, Poisson's ratio ν = 0.14±0.02 and material density ρ = (1.7±0.05)·10^3 kg/m^3.

As shown by the derived dependencies, the best convergence between them is observed for circular defect radius in the range of 6–18 mm, which corresponds to subsurface defects Nos 2–5.

Despite that, research results are indicative of the applicability of formula (2) to determine the depth of defect occurrence with sufficient accuracy in the entire studied range. Deviation of experimental results from the theoretical ones shown in Figure 5, are attributable, in particular, to imperfection of formula (2) for determination of the main resonance frequency f_{01}, deviations in the dimensions of the introduced defects, material orthotropy, etc. One of the methods to improve the accuracy of establishing the parameters of a subsurface defect of unknown dimensions and depth of occurrence is determination of not just the fundamental resonance frequency f_{01}, but also higher order frequencies. Having experimentally determined these frequencies and using formula (2), as well as the respective coefficients for finding multiple resonance frequencies for an isotropic material, we can experimentally determine these resonance frequencies by the spatial structure of optical responses, and, thus, determine the depth of the defect occurrence at unchanged parameters of the composite plate surface layer. Note that for a circular subsurface defect, the spatial structure of optical responses at the fundamental and multiple resonance frequencies corresponds to the structure of the nodes and antinodes of a circular membrane of the same diameter, and that of the defect, at the same resonance frequencies.

Thus, the results of studying the circular subsurface defects using OAS layout and derived experimental dependence of resonance frequency f_{01} on defect radius *a* at depth of occurrence h = 0.41 mm testify to the fundamental possibility of evaluation of the subsurface defect area and its geometrical dimensions.

CONCLUSIONS

Based on the developed OAM, OAS layout was created, which enables detection of subsurface defects in composite laminated structures using a series of dynamic speckle patterns of the composite layer surface above the defect, excited by a flexural elastic wave. After their recording, difference DSP are formed and optical spatial responses from the defects are detected in case of their presence in the digital camera field of view. Formation of dynamic speckle patterns does not require application of an additional reference beam in OAS, which enables designing on its base high-speed optical-digital devices for NDT of subsurface defects, with a low sensitivity to vibrations or other external factors and which are capable of operation in site. It is shown that difference DSP derived at fundamental resonance frequencies f_{01} for circular subsurface defects, allow detecting these defects in fiberglass laminated structures and determining their sizes with diameters in the range of 8–45 mm.

REFERENCES

1. Newman, J.W. (2012) *Laser testing: Shearography & Holography*. Ed. by P.O. Moore. The Nondestructive Testing Overview, Columbus Ohio, American Society for Nondestructive Testing.
2. Lobanov, L.M., Pivtorak, V.A. (2014) Diagnostics of structures by the methods of electron shearography and speckle-interferometry. *Materials Sci.*, **49**, 442–448. DOI: https://doi.org/10.1007/s11003-014-9635-5
3. Howell, P.A. (2020) *Nondestructive evaluation (NDE) Methods and capabilities:* Handbook, NASA/TM−2020-220568, Vol I. Langley Research Center, Hampton, VA, USA.

4. Nazarchuk, Z, Muravsky, L., Kuryliak, D. (2023) Digital speckle pattern interferometry for studying surface deformation and fracture of materials. In*: Optical Metrology and Optoacoustics in Nondestructive Evaluation of Materials*. Springer Series in Optical Sciences, **242**. Singapore: Springer, 149–217. DOI: https://doi.org/10.1007/978-981-99-1226-1_4
5. Chatters, T., Pouet, B., Krishnaswamy, S. (1992) *Shearography with synchronized pressure stressing*. Eds by D.O. Thompson, D.E. Chimenti, Review of Progress in Quantitative NDE, La Jolla, CA, Plenum Press, 426. DOI: https://doi.org/10.1007/978-1-4615-2848-7_54
6. Hung, Y.Y., Yang, L.X., Huang, Y.H. (2013) Nondestructive evaluation (NDE) of composites: Digital shearography. Ed. by V.M. Karbhari, In: *Nondestructive evaluation (NDE) of polymer matrix composites*. Cambridge, Philadelphia, New Delhi: Woodhead Publishing Limited, 84–115.
7. Muravsky, L., Kuts, O., Gaskevych, G., Suriadova, O. (2019) Detection of subsurface defects in composite panels using dynamic speckle patterns. In: *Proc. of IEEE XIth Inter. Scientific and Practical Conf. on Electronics and Information Technologies, 2019*, 7–10. DOI: https://doi. org/10.1109E/LIT.2019.8892294
8. Nazarchuk, Z., Muravsky, L., Kuryliak, D. (2019) To the problem of the subsurface defects detection: Theory and experiment. *Procedia Structural Integrity*, **16**, 11–18. DOI: https://doi.org/10.1016/j.prostr.2019.07.016
9. Nazarchuk, Z.T., Muravsky, L.I., Kuts, O.G. (2022) Nondestructive testing of thin composite structures for subsurface defects detection using dynamic laser speckles. *Research in Nondestructive Evaluation,* **33**, 59–77. DOI: https://doi.org/10.1080/09349847.2022.2049407
10. Muravsky, L., Nazarchuk, Z., Kuts, O., Sharabura, O. (2023) Identification of internal planar square defects in composite panels using optoacoustic technique. In*: Proc. of IEEE 13th Inter. Conf. on Electronics and Information Technologies, ELIT 2023*, 265–269. DOI: https://doi. org/10.1109/ELIT61488.2023.10310846
11. Nazarchuk, Z., Muravsky, L., Kuryliak, D. (2023) Methods for processing and analyzing the speckle patterns of materials surfaces. In*: Optical metrology and optoacoustics in nondestructive evaluation of materials*. Springer Series in Optical Sci., **242**. Singapore: Springer, 249–323. DOI: https://doi.org/10.1007/978-981-99-1226-1_6
12. Timoshenko, S.P., Woinowsky-Krieger, S. (1959) *Theory of plates and shells*. 2nd Ed., McGraw-Hill, New York.
13. Leissa, A.W. (1969) *Vibration of plates*. Scientific and Technical Information Division, National Aeronautics and Space Administration.
14. Li, W.L. (2004) Vibration analysis of rectangular plates with general elastic boundary supports. *J. of Sound and Vibration*, 273(**3**), 619–635. DOI: https://doi.org/10.1016/S0022-460X(03)00562-5
15. Guguloth, G.N., Singh, B.N., Ranjan, V. (2019) Free vibration analysis of simply supported rectangular plates. *Vibroengineering Procedia*, **29**, 270–273. DOI: https://doi.org/10.21595/vp.2019.21135
16. Chakraverty, S., Jindal, R. Agarwal, V.K. (2007) Effect of non-homogeneity on natural frequencies of vibration of elliptic plates. *Meccanica,* **42**, 585–599. DOI: https://doi.org/10.1007/s11012-007-9077-3
17. Maiz, S., Rossit, C.A., Bambill, D.V., Susca, A. (2009) Transverse vibrations of a clamped elliptical plate carrying a concentrated mass at an arbitrary position. *J. of Sound and Vibration*, 320(**4–5**), 1146–1163. DOI: https://doi. org/10.1016/j.jsv.2008.09.013
18. Zhou, Z.H., Wong, K.W., Xu, X.S., Leung, A.Y.T. (2011) Natural vibration of circular and annular thin plates by Hamiltonian approach. *J. of Sound and Vibration*, 330(**5**), 1005–1017. DOI: https://doi.org/10.1016/j.jsv.2010.09.015
19. Anjomshoa, A., Tahani, M. (2016) Vibration analysis of orthotropic circular and elliptical nano-plates embedded in elastic medium based on nonlocal Mindlin plate theory and using Galerkin method. *J. of Mechanical Sci. and Technology*, **30**, 2463–2474. DOI: https://doi.org/10.1007/ s12206-016-0506-x
20. Cawley, P. (1984) The impedance method of nondestructive inspection. *NDT Inter.*, **17**(2), 59–65. DOI: https:// doi.org/10.1016/0308-9126(84)90045-2
21. Cawley, P., Theodorakopoulos, C. (1989) The membrane resonance method of nondestructive testing. *J. of Sound and Vibration*, 130(**2**), 299–311. DOI: https://doi. org/10.1016/0022-460X(89)90555-5
22. Ma, C.C., Huang, C.H. (2004) Experimental whole-field interferometry for transverse vibration of plates. *J. of Sound and Vibration,* 271(**3–5**), 493–506. DOI: https://doi. org/10.1016/S0022-460X(03)00276-1
23. Bruno, F., Laurent, J., Prada, C. et al. (2014) Nondestructive testing of composite plates by holographic vibrometry. *J. of Applied Physics*, 115(**15**), 154503. DOI: https://dx.doi.org/10.1063/1.4871178
24. Lamboul, B., Giraudo, O., Osmont, D. (2015) Detection of disbonds in foam composite assemblies using flexural waves and shearography. In: *AIP Conf. Proceedings,* 1650(**1**), 1155–1161. DOI: http://dx.doi.org/10.1063/1.4914725

ORCID
O.M. Sharabura: 0000-0002-5712-4114,
L.I. Muravsky: 0000-0001-8839-2819

CONFLICT OF INTEREST
The Authors declare no conflict of interest

CORRESPONDING AUTHOR
L.I. Muravsky
G.V. Karpenko Physico-Mechanical Institute of the NASU
5 Naukova Str., 79060, Lviv, Ukraine.
E-mail: muravskyleon@gmail.com

SUGGESTED CITATION
O.M. Sharabura, L.I. Muravsky, O.G. Kuts (2025) Detection of circular subsurface defects in laminated composites using optical-acoustic nondestructive testing system. *The Paton Welding J.*, **2**, 42–46. DOI: https://doi.org/10.37434/tpwj2025.02.07

JOURNAL HOME PAGE
https://patonpublishinghouse.com/eng/journals/tpwj

Received: 24.10.2024
Received in revised form: 14.11.2024
Accepted: 31.03.2025